Precision Engineering 52 (2018) 356–369

Contents lists available at ScienceDirect

Precision Engineering

journal homepage: www.elsevier.com/locate/precision

Material removal mechanism and surface integrity in ultraprecision cutting of porous titanium

Mehdi Heidari, Jiwang Yan*

Department of Mechanical Engineering, Keio University, Hiyoshi 3-14-1, Kohoku-ku, Yokohama, 223-8522, Japan

ARTICLE INFO

Keywords:
Porous titanium
Ultraprecision cutting
Diamond turning
Chip formation
Surface integrity
Tool wear

ABSTRACT

Porous titanium presents unique material properties with a wide variety of mechanical and biomedical applications. Porous titanium components fabricated by near net-shape technologies require further machining processes to improve the surface quality and form accuracy, and in turn, the added value of the products. In this work, major factors dominating the surface integrity in ultraprecision cutting of porous titanium using single-crystal diamond tools were investigated. The results demonstrated that the presence of pores significantly changed mechanism of cutting. The chip morphology and surface topography depended on pore size and undeformed chip thickness. At an extremely small undeformed chip thickness, a majority pores were closed due to the welding phenomenon, leading to a sharp drop of surface porosity. In contrast, large pores cause craters on the machined surface and segmentation of chips and protruding lamella, especially at a large undeformed chip thickness. A coolant could lubricate the tool-workpiece interface and the shear deformation, which decreased cutting forces. On the other hand, the rapid cooling effect enhanced the work hardening effect and increase the hardness of the machined surface. Tool wear in cutting porous titanium is suppressed compared with that of pure titanium, especially in wet cutting.

1. Introduction

Titanium is an attractive material due to its unique properties such as high strength, light weight, thermal stability, and exceptional corrosion resistance. These excellent properties make titanium and its alloys useful in biomedical, chemical and petrochemical applications and aerospace and marine industries. With the introduction of metal foams in medical technology within the last decades, porous titanium has received great interest. Porous titanium is a potential material for various dental and orthopedic applications due to its excellent biocompatibility properties. In biomedical applications, in addition to requirements for complex shapes, surface integrity, microstructure, and porosity significantly influence the adherence between an implant and a neighboring bone, as well as their biocompatibility [1–3]. High-precision fabrication technologies, such as ultraprecision cutting, are expected to meet these requirements and open new technological possibilities for manufacturing this class of products.

A few researches have been carried out on the cutting mechanism of porous titanium. Abolghasemi Fakhri et al. [1] proposed an image analysis approach to optically consider the porosity in milling process of porous titanium, with emphasis on cutting force monitoring. The result showed the possibility of estimating the area of porous material removal from the optical image. Bram et al. [4] monitored cutting force during grinding and face milling of sintered titanium foam to investigate the surface quality and tool wear. However, to date, there is no available literature on the mechanism of cutting of porous titanium at a maximum undeformed chip thickness of submicron level or smaller.

In an extremely small machining scale, the machining mechanism of a porous material is distinctly different from that of a non-porous continuous material. Chen et al. [5] investigated the effects of tool geometry, tool material properties and machining parameters on the surface porosity of porous tungsten. Schoop et al. [6] machined porous tungsten and tried to control brittle microfracture to obtain a suitable surface porosity. Pusavec [7] used a multi-objective optimization model based on genetic algorithms to achieve the best machining performance in porous tungsten cutting under cryogenic conditions by predicting the optimal input cutting parameters. In a previous study by the present authors, diamond turning experiments of porous silicon have been performed to investigate the fundamental mechanisms of material removal and surface formation. The results showed the possibility of generating a nanometer-level surface flatness with open pores [8]. In addition, the possibility of diamond turning porous carbon for direct fabrication of precision air bearing surfaces was demonstrated [9].

* Corresponding author.
E-mail address: yan@mech.keio.ac.jp (J. Yan).

https://doi.org/10.1016/j.precisioneng.2018.01.014
Received 31 October 2017; Received in revised form 6 January 2018; Accepted 18 January 2018
Available online 31 January 2018
0141-6359/

Table 1
Chemical compositions of porous titanium.

Purity%	Fe%	O%	C%	N%	H%
99.8	0.04–0.25	0.1–0.2	0.0–0.08	0.0–0.03	0.01–0.13

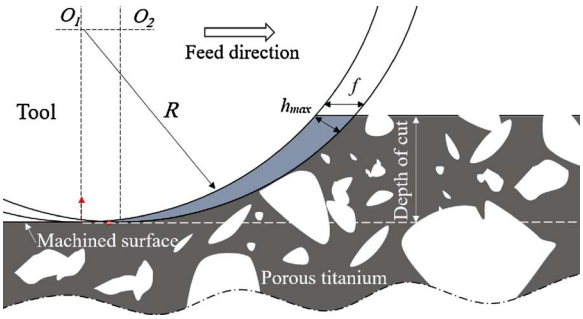

Fig. 2. Cutting model for a round-nosed tool.

Table 2
Machining conditions.

Depth of cut *(a)*	5, 15 μm
Feed rate *(f)*	1, 10, 50, 100 μm/rev
Cutting speed *(v)*	50 m/min
Spindle rotation *(n)*	252–176 rpm
Maximum undeformed chip thickness (h_{max})	99–12331 nm

In this study, the cutting mechanism and surface integrity in ultra-precision machining of porous titanium have been investigated and compared with those of pure titanium. For this purpose, the effects of cutting parameters, coolants, and pore size on chip formation, surface topography, surface hardness, and tool wear have been studied. The key factors affecting the machined surface integrity of porous titanium have been identified. The findings from this study will establish process criteria for the ultraprecision manufacturing of porous titanium functional products for biomedical applications, and so on.

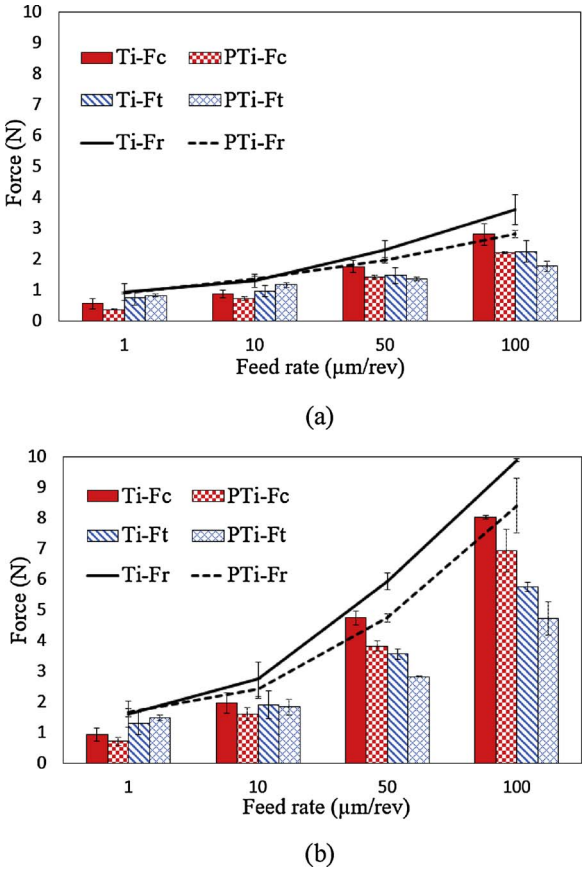

Fig. 3. Cutting forces of pure titanium (Ti) and porous titanium (PTi) in dry condition at depth of cut (a) 5 μm and (b) 15 μm.

2. Experimental and simulation procedures

2.1. Material

Porous titanium blocks (sample size: 20.0 mm × 15.0 mm × 10.0 mm) with purity of 99.8% were used as workpiece. For comparison, pure

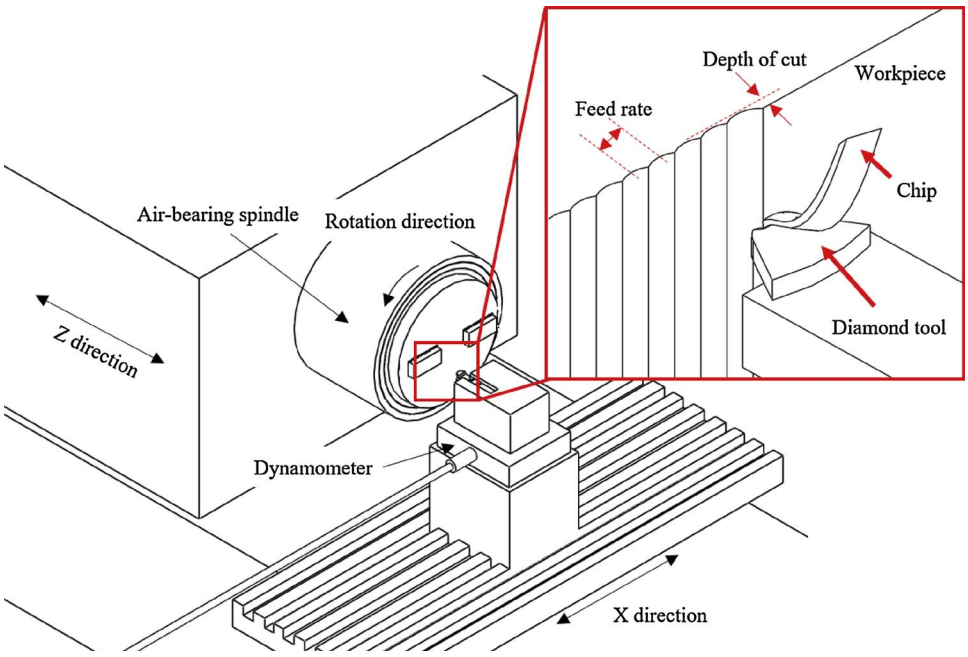

Fig. 1. Schematic diagram of experimental setup.

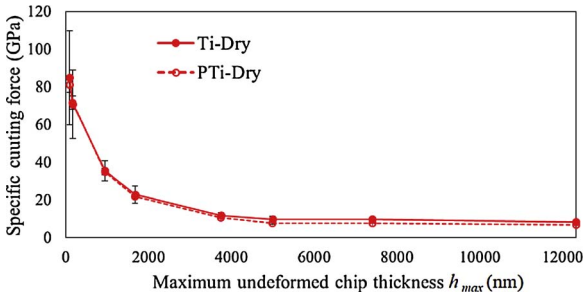

Fig. 4. Changes of specific cutting force with $h_{max.}$

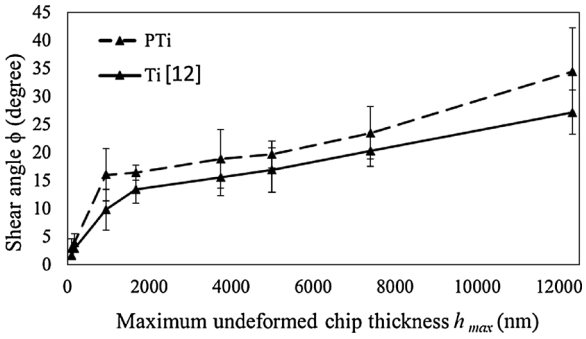

Fig. 5. Changes of shear angle with $h_{max.}$

titanium blocks with the same size were also machined. The chemical compositions of both pure titanium and porous titanium were the same, as shown in Table 1. The porosity of the porous titanium samples used in the experiments was ~30%, with pore size ranging from a few nanometers to ~100 μ. The titanium sample has ultimate tensile strength of 370 MPa, yield strength of 300 MPa and hardness of 145 HV.

2.2. Experimental setup

Face turning was performed using a three-axis control ultraprecision machine, NACHI ASP-15 (NACHI-FUJIKOSHI CORP). The machine has two perpendicular linear tables supported by high-stiffness hydrostatic bearings driven by servomotors. To prevent from backlash movements in machine rotary table, it is supported by hydrostatic bearings and driven by a friction drive. The machine is equipped with laser hologram scales to accurately position all of these tables. The linear tables can be moved at 1 nm per step and the rotary table is able to rotate with an angular resolution of 0.00001°. A piezoelectric dynamometer (Kistler 9256C2) was mounted below the tool holder to measure cutting forces during the cutting tests. Fig. 1 shows a schematic diagram of the experimental setup.

A workpiece holder was designed and fabricated to fix the workpiece to the spindle using a sliding mechanism to adjust the distance between the workpiece and the center of the spindle. The workpiece was fixed using three screws to the holder which is then vacuum chucked to the machine spindle. A metal piece was fixed on the opposite side of the workpiece to keep dynamic balance during spindle rotation. To guarantee the accuracy of results, all machining tests were repeated twice at the same conditions.

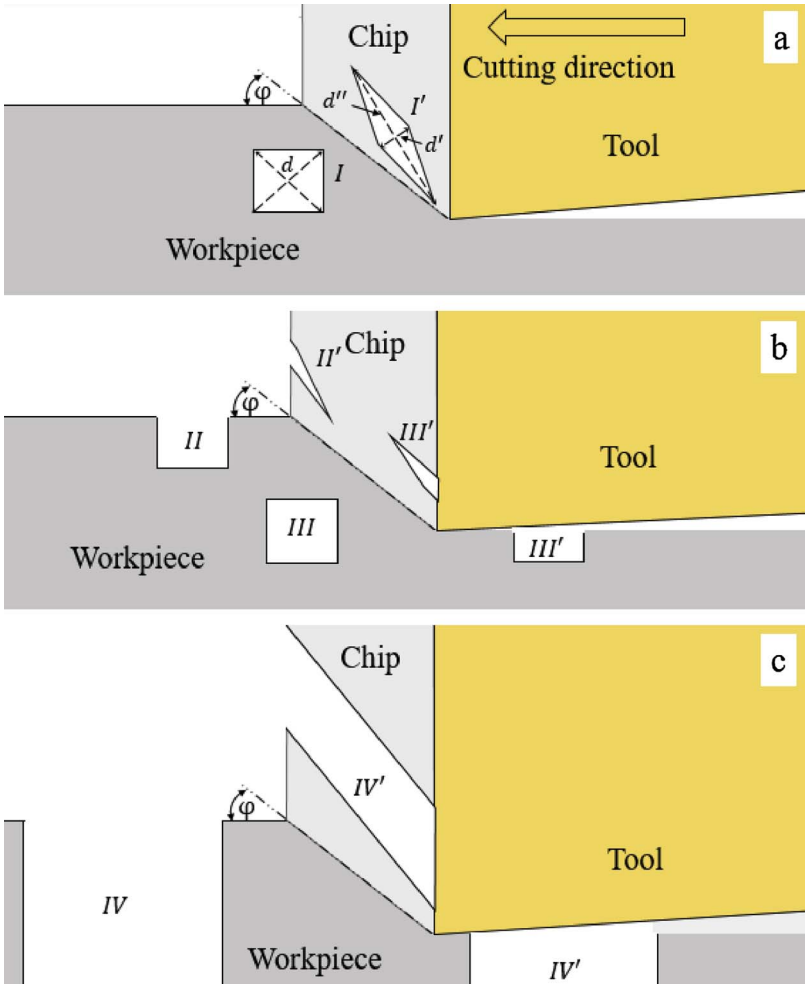

Fig. 6. Schematic illustration of pore deformation in cutting porous titanium.

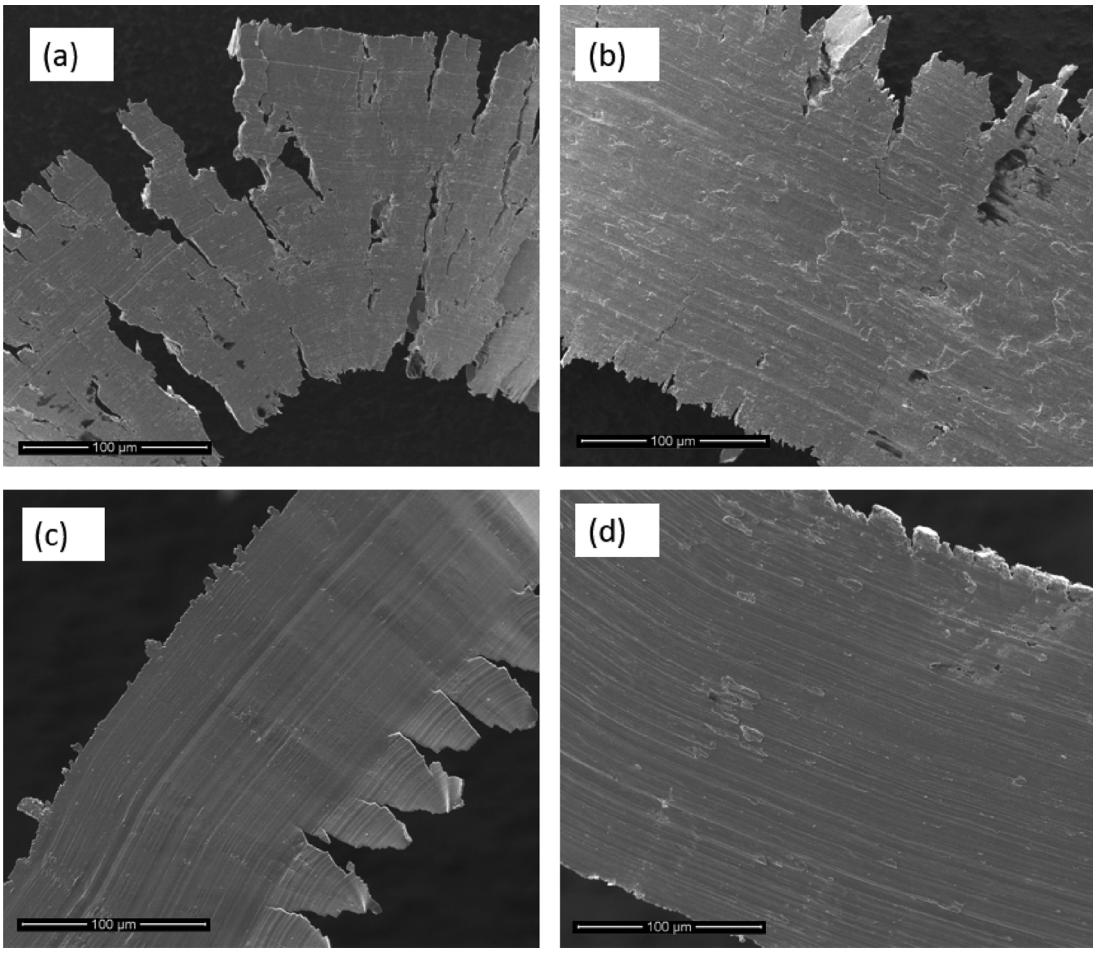

Fig. 7. SEM micrographs of back sides of chips at (a) h_{max} = 1676 nm, (b) h_{max} = 12331 nm in cutting porous titanium, and (c) h_{max} = 1676 nm, (d) h_{max} = 12331 nm in cutting pure titanium.

In order to evaluate the machined surface texture, a white light interferometer was used and the surface profile was analyzed by the Talymap software (Taylor Hobson Ltd.). A scanning electron microscope (SEM, Model Inspect S50) was used to observe the chips, the machined surfaces and tool wear. SEM images of the machined surface were then used for analyzing the surface porosity using the ImageJ software. To evaluate surface hardness variations, hardness measurements were performed using a micro Vickers hardness tester (Shimadzu HMV-G21S) by applying a load of 1 N for 10 s on selected specimens.

2.3. Cutting tool and cutting model

In this study commercially available single-crystal diamond tools with a nose radius of 1.0 mm, rake and clearance angles of 0° and 6°, respectively, were used in the experiments. In ultraprecision diamond turning with a round-nosed tool, the maximum undeformed chip thickness (h_{max}) is an important parameter to evaluate the cutting performance. Fig. 2 shows a schematic model for diamond turning with a round-nosed tool. $h_{\max}$ can be calculated from the tool nose radius R, depth of cut a and tool feed rate f, using the following equation when $f < \sqrt{2Ra - a^2}$ [10,11].

$$h_{max} = R - \sqrt{R^2 + f^2 - 2f\sqrt{2Ra - a^2}} \quad (1)$$

When $f \geq \sqrt{2Ra - a^2}$, however, $h_{\max}$ is equal to the depth of cut (a).

2.4. Machining parameters

Four feed rates and two depths of cut were used to cut concentric areas on each sample. Since the distance of each area from the spindle center is different, spindle rotation rate was adjusted for each area to get the same cutting speed in all tests. Table 2 shows the machining parameters of experiments. In addition, experiments were performed under dry cutting conditions and wet conditions using a coolant, respectively. As coolant, CASTY-LUBE® B-905, a fatty acid ester, with a density of 0.8782 (15 °C) g/cm^3 was used in the form of mist jet.

2.5. Finite element simulation

To assist understanding the material removal mechanism of porous titanium, the material deformation in the cutting area was simulated by using AdvantEdge, a finite element (FE) machining simulation program produced by Third Wave Systems USA. Two-dimensional simulations of orthogonal cutting were performed, thus, the undeformed chip thickness was the same as the depth of cut. The tool rake angle, relief angle and cutting speed used in the simulations were the same as those used in the experiments. Using a tool edge radius (r) smaller than 100 nm, as used in the experiment, was extremely time-consuming in simulations, so an edge radius of 400 nm was used. Accordingly, depth of cuts (a) were also enlarged in the simulation to keep the same proportion of depth of cut to edge radius as that in experiments. The coefficient of friction between tool rake face and chip used in the FE simulations was 0.7, which was obtained from in micrometer scale cutting experiments of titanium. For workpiece and tool meshing, the minimum element size was set to 100 nm. The mechanical properties such as ultimate tensile strength, yield strength and hardness used in the simulations were the same as those of as-received titanium samples. The modified power law constitutive model, which was defined by the AdvantEdge

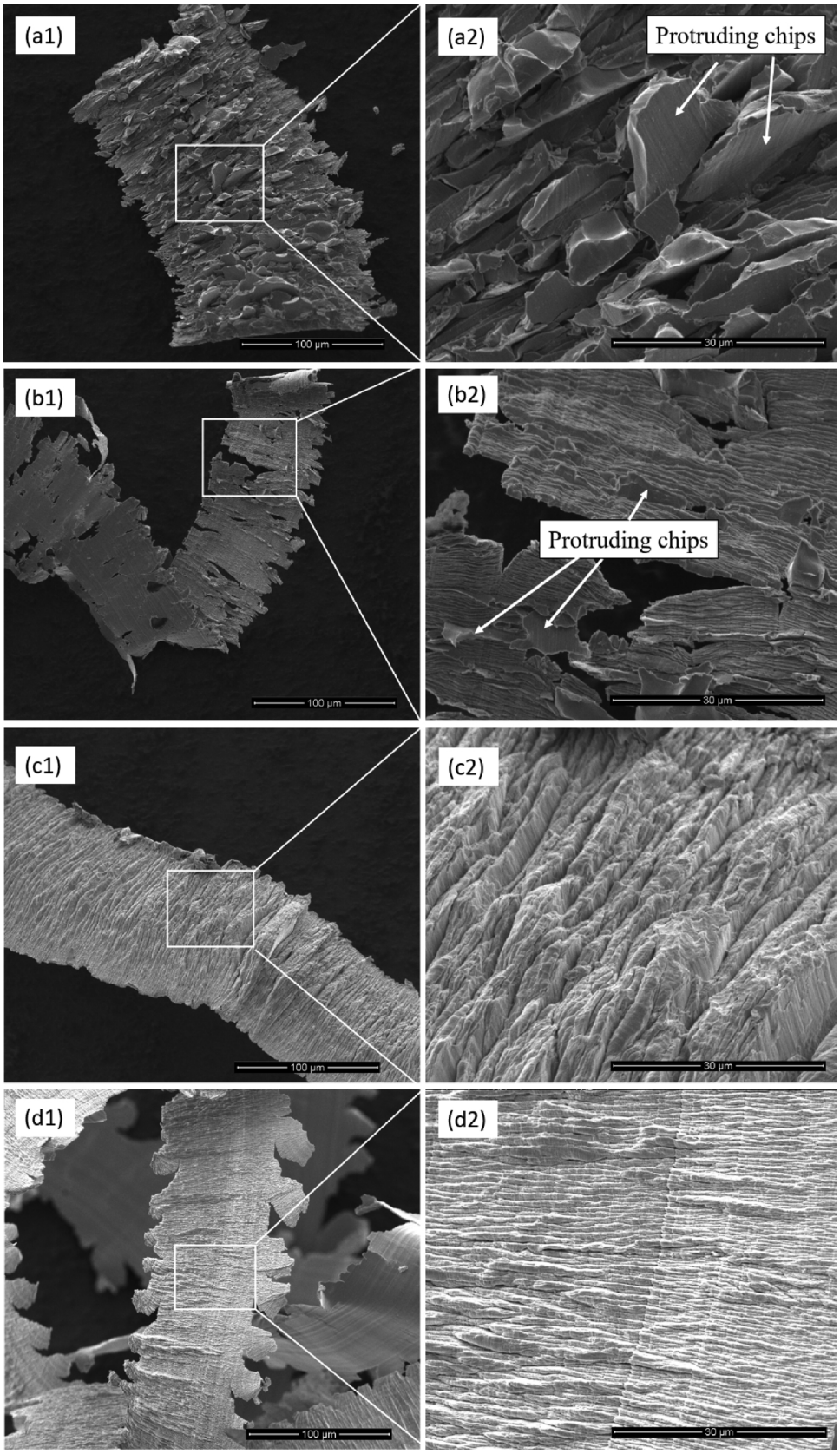

Fig. 8. SEM micrographs of chips generated in porous titanium cutting at (a) h_{max} = 4999 nm and (b) h_{max} = 949 nm. For comparison, chips generated in pure titanium cutting at (c) h_{max} = 4999 nm and (d) h_{max} = 949 nm are also shown.

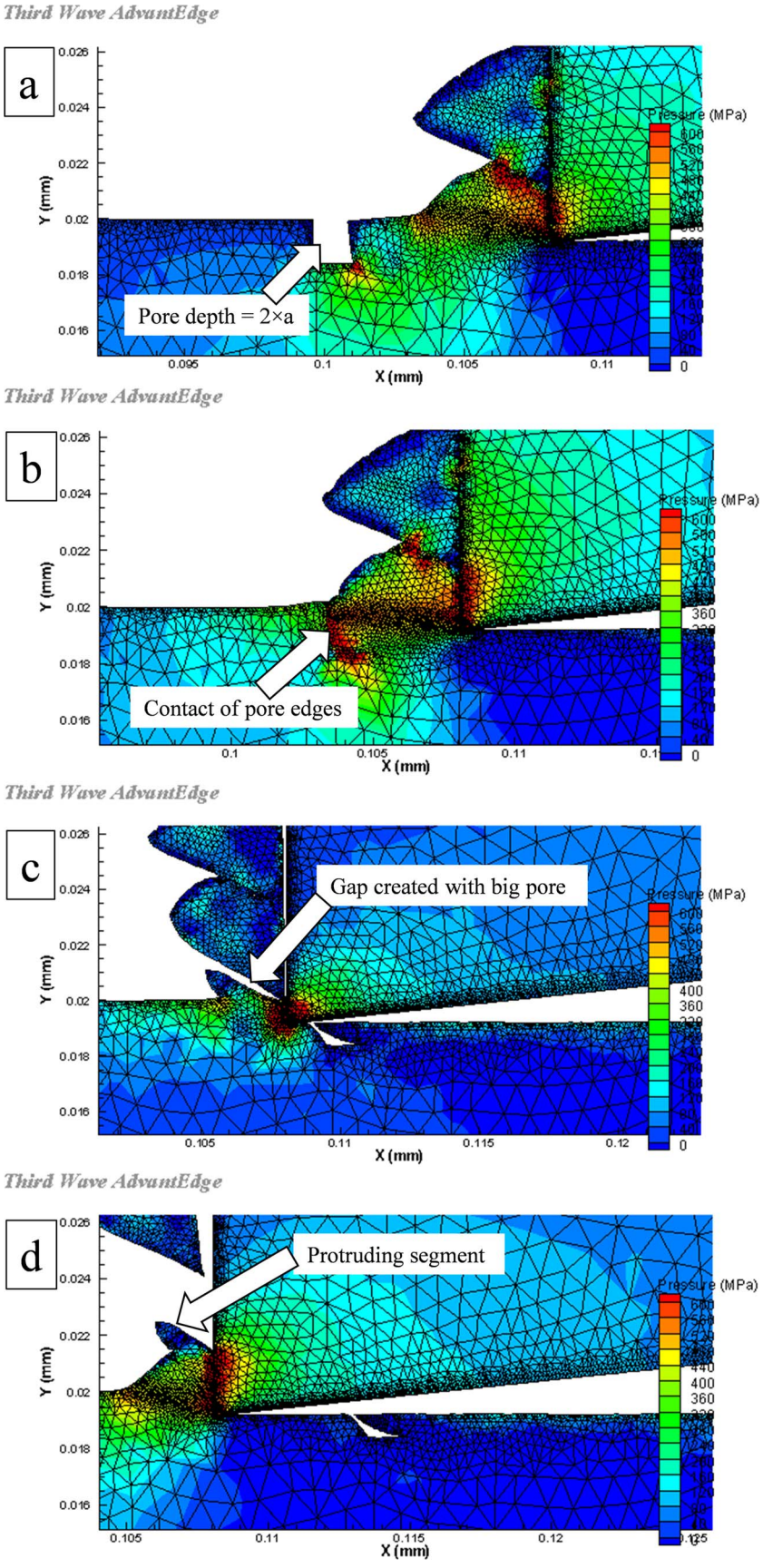

Fig. 9. FE simulations of chip formation behavior near a pore ($a = 2r$).

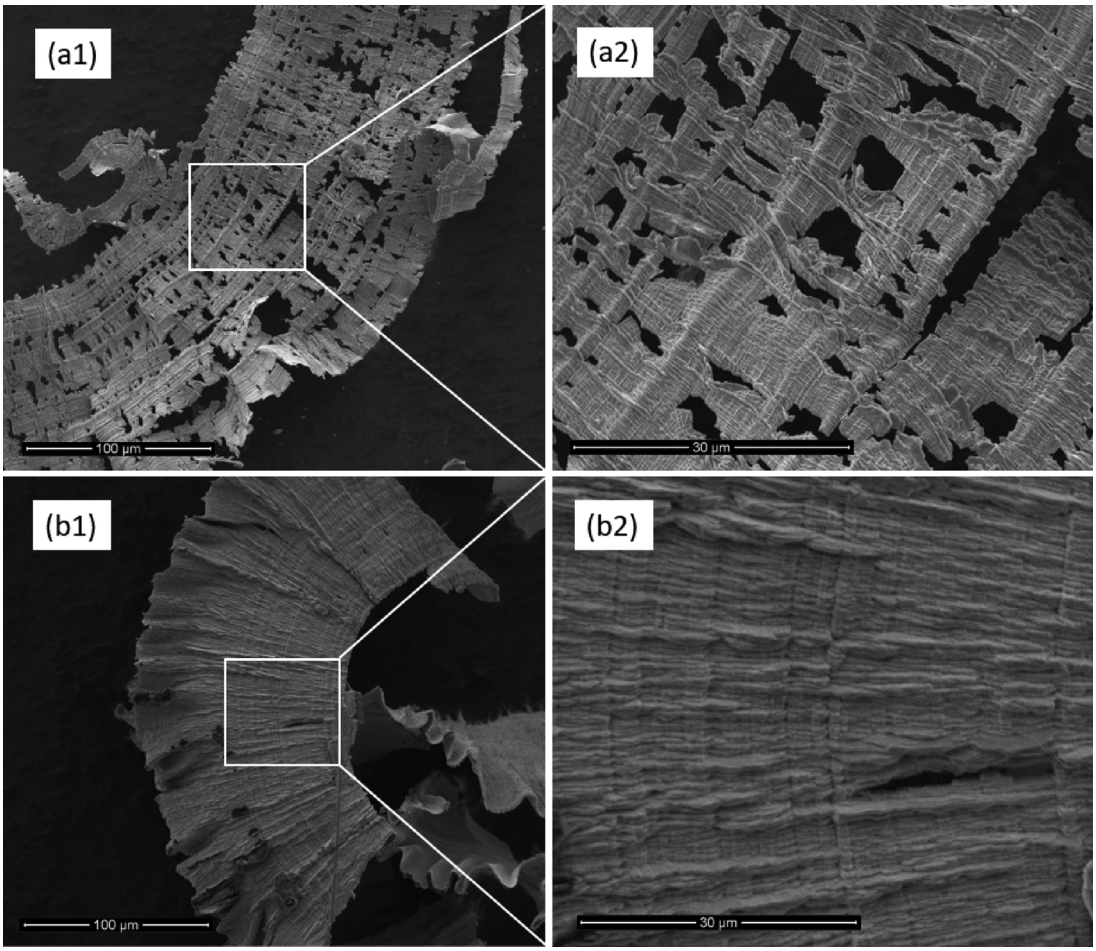

Fig. 10. SEM micrographs of front sides of chips of (a) porous titanium and (b) pure titanium at the same undeformed chip thickness (h_{max} = 172 nm).

software, was used as the stress-strain constitutive of workpiece material.

3. Results and discussion

3.1. Cutting force characteristics

Fig. 3 shows the principal force (F_c), thrust force (F_t) and resultant force (F_r) during machining titanium (Ti) and porous titanium (PTi) at two depth of cuts.

The figure indicates the decrease of resultant force as feed rate decreases. There is also an increase in cutting forces as depth of cut increases from 5 to 15 µm. Comparison of cutting forces between pure titanium and porous titanium shows that, although the magnitude of cutting forces of pure titanium is about 15% greater than that of porous titanium at a high feed rate (100 µm/rev) and depth of cut (15 µm), this percentage becomes zero at a low feed rate (1 µm/rev). The gap in cutting force between pure titanium and porous titanium is caused by the pores which reduces the effective volume of deformed material.

Fig. 4 shows the results of specific cutting force with respect to h_{max}. As h_{max} decreases, the specific cutting force increases slightly in the micro level, and then sharply when h_{max} approaches the submicron level. The sharp rise in specific cutting force at an extremely small undeformed chip thickness contributes to chip tearing phenomenon in pure titanium cutting [12]. As the ratio between the undeformed chip thickness and the tool edge radius decreases, the size effect in specific cutting force is predominant, as known in traditional metal cutting [13–20]. Decreasing this ratio also leads to an increase in fluctuation of specific cutting force, as shown in Fig. 4, due to the pores and saw-toothed chip formation. The specific cutting force in porous titanium cutting is slightly lower than that in pure titanium cutting due to the existence of pores and the different disappear as h_{max} decreases.

3.2. Chip morphology

Next, the shear angle φ, which is defined as the angle between the shear plane and the cutting direction, was derived from arctangent of the ratio (r_c) of undeformed chip thickness (h) to the chip thickness (l), which were experimentally measured from SEM photographs of the chips, as shown in Fig. 5. Although the shear angle for porous titanium demonstrates a similar trend to that for pure titanium workpiece with respect to undeformed chip thickness, the shear angle of porous titanium is larger than that of pure titanium. The difference of shear angle is ~10° under the present conditions.

The significant difference in shear angle between pure titanium and porous titanium is due to the presence of pores. This difference can be explained based on deformation process of pores in the shear zone.

The presence of pores causes the edge-induced stress to be released as it reaches a pore leading to decreasing specific cutting force down to 20% in micro-scale cutting as it is already shown in Fig. 4. Decreasing specific cutting force is the main reason of increasing shear angle in porous titanium cutting [21,22]. However, as undeformed chip thickness decreases to the nanometer scale, shear angle gap vanishes and specific cutting force increases due to the welding phenomenon (see more in Section 3.3).

The pores can be divided into two categories respecting to their

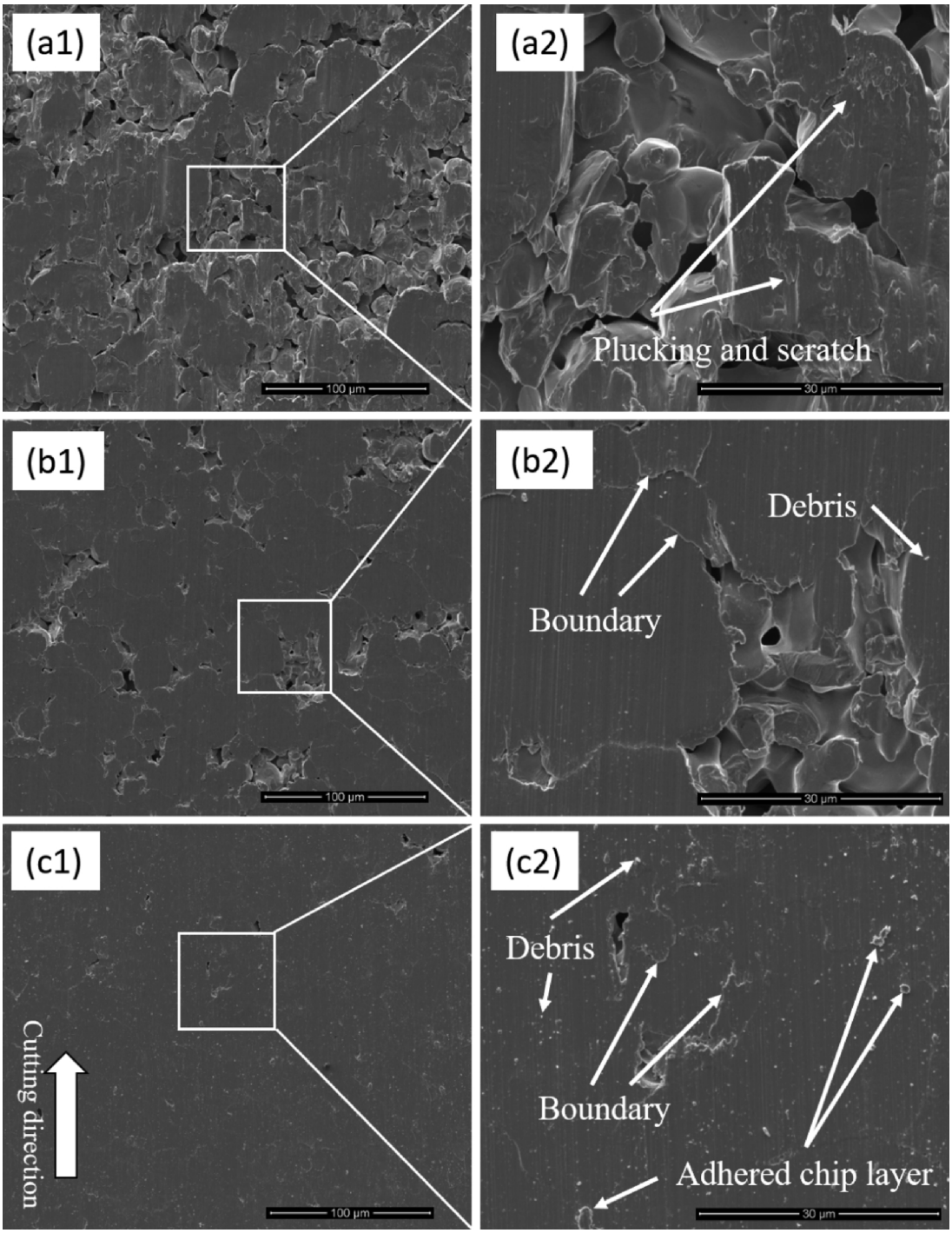

Fig. 11. SEM micrographs of machined surface of porous titanium at (a) h_{max} = 12331 nm, (b) h_{max} = 1676 nm, and (c) h_{max} = 172 nm.

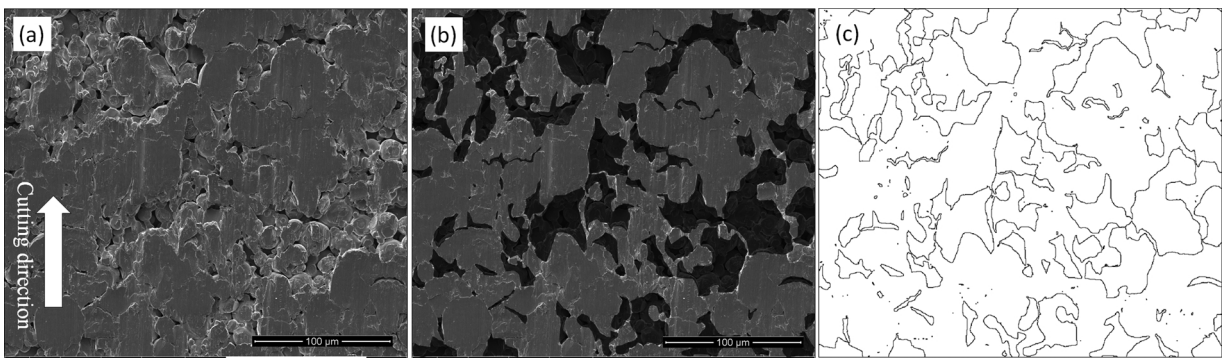

Fig. 12. Image-processed results for calculating surface porosity on the machined surface of porous titanium at h_{max} = 12331 nm.

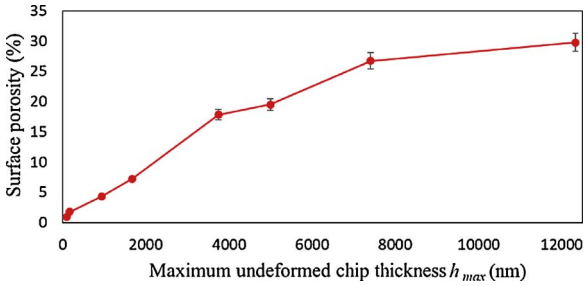

Fig. 13. Change of porosity percentage with h_{max}.

sizes: pores smaller than undeformed chip thickness and pores bigger than undeformed chip thickness, the ratio of which decreases as undeformed chip thickness decreases.

Fig. 6 is a schematic illustration of the deformation process of pores in porous titanium cutting. A square element is used to present a pore, which is deformed into a rhombus after passing through the shear plane. Fig. 6a shows the deformation of a pore with size less than undeformed chip thickness. The pore is remained inside the chip after deformation, and the ratio of *d' to d*", which indicates pore close, decreases with the shear angle. Thus, the pores with size less than undeformed chip thickness tend to be closed due to shear deformation. The possibility of air entrainment in the chip is very low owing to the fact that most of the pores in porous titanium are interconnected. The effect of pores also depends on the depth of pore in the workpiece. Fig. 6b illustrates two pores with the same size as that in Fig. 6a but at two different locations. For the pore near the workpiece as indicated by "II", the pore remains in the chip as an opening on the chip surface; while for the deeper pore indicated by "III", the bottom part remains on machined surface leading to an open cavity on the surface, and the top part causes an opening on the back side of the chip. In addition to the effect of shear deformation on deformation of pore, the chip-tool friction has profound influences on the deformation of pore, as indicated by pore "III". Interface friction in chip-tool contact zone causes the top part of pore "III" to be closed. Where a pore is very large, as indicated by pore "IV" in Fig. 6c, the pore not only causes a big opening on the machined surface but also leads to chip segmentation.

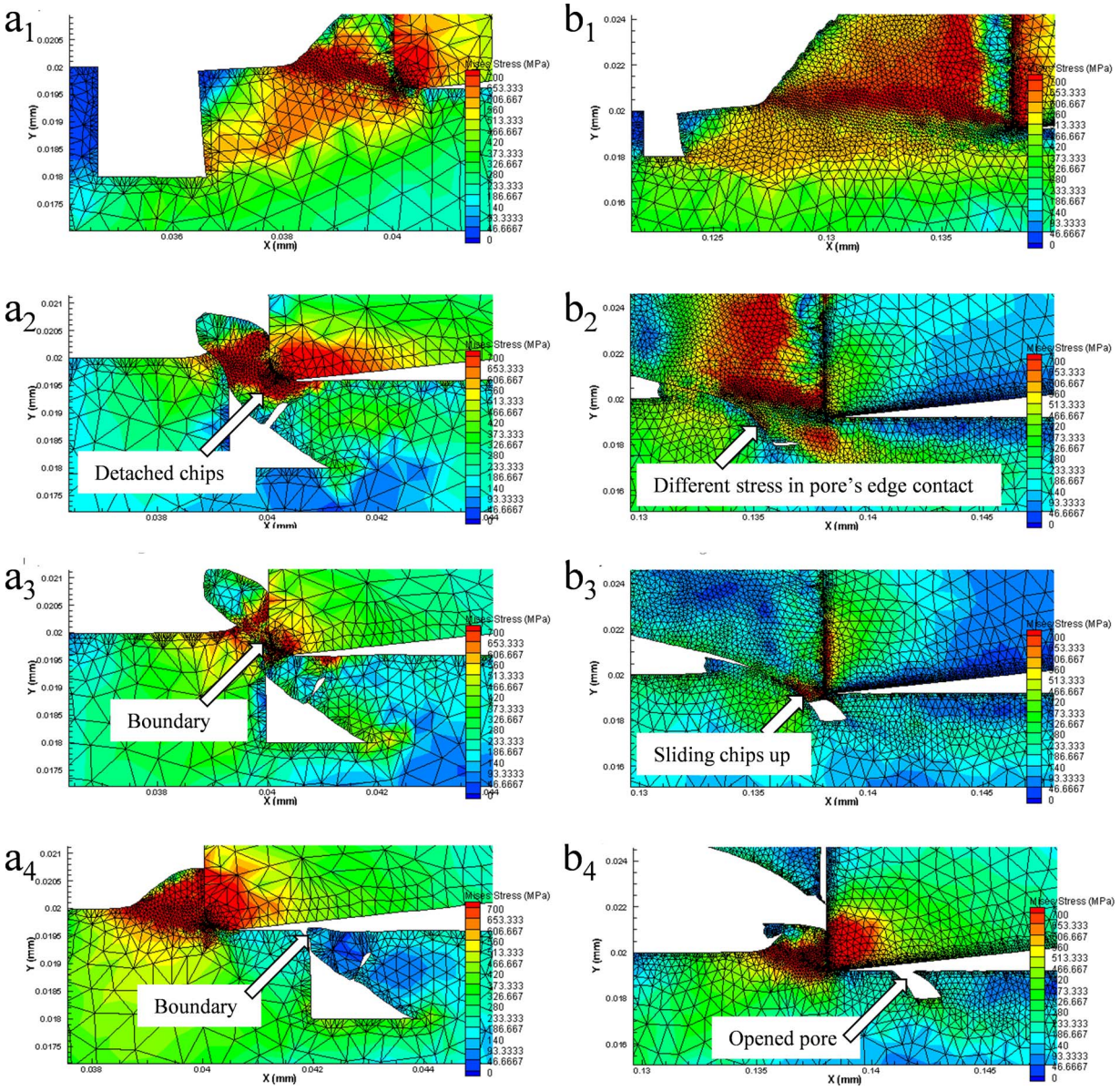

Fig. 14. FE simulations of cutting behavior near pores (Mises stress) at (a) $a = r$ and (b) $a = 2r$.

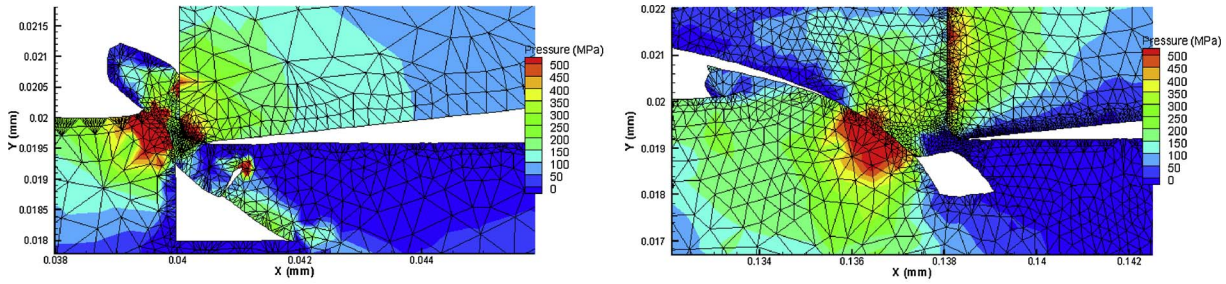

Fig. 15. FE simulations of cutting behavior near pores (Pressure) at (a) $a = r$ and (b) $a = 2r$.

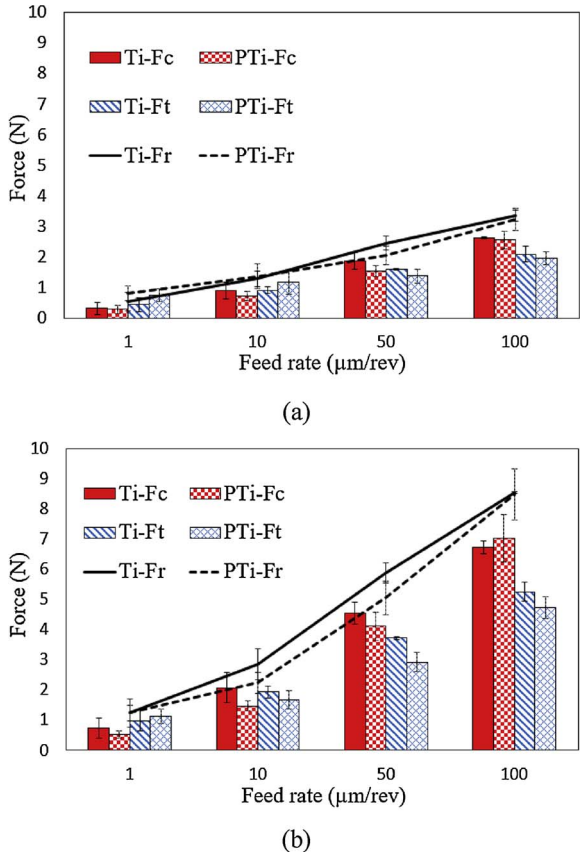

Fig. 16. Cutting forces of pure titanium (Ti) and porous titanium (PTi) in wet condition at depth of cut (a) 5 μm and (b) 15 μm.

Fig. 7a and b show the back sides of chips generated in the cutting of porous titanium in comparison with chips generated in cutting of pure titanium (Fig. 7c and d). It is clear that the chips of pure titanium have very smooth surfaces, whereas those of porous titanium are rougher and contain many opening pores and chip tearing phenomenon found in pure titanium cutting (Fig. 7c) [12] takes place at a small h_{max} for porous titanium too (Fig. 7a). Compared to pure titanium chips (Fig. 7c), the porous titanium chips are torn more significantly (Fig. 7a), indicating that the presence of pores increases the possibility of chip tearing.

Differences were also confirmed on the front sides of the chips. As shown in Fig. 8, the chips of porous titanium have sharp segments protruding from the surface. This kind of chip segmentation might have been caused by the big pores indicated by "IV" in Fig. 6c. The pores induce big gaps inside chips which terminates shear deformation of the material. As a result, the chip will be segmented and the material will protrude out of the gap without shear deformation. Although, the segment protruding phenomenon does not occur on the back side of the chip due to chip-tool friction. The protruding chips are distinguished from the regularly segmented chips by the features that the protruding chips are generated randomly and separated with each other; whereas for the regularly segmented chips, the lamella structures are long and uniform along the chip width. By comparing Fig. 8a and b, it is seen that the chip segment protruding phenomenon becomes insignificant as undeformed chip thickness decreases. For pure titanium, however, as shown in Fig. 8c and d, the chips have regular lamella structure without segment protrusion.

Table 3
Vicker hardness (HV) of machined surface.

	a	f			
		1 μm/rev	10 μm/rev	50 μm/rev	100 μm/rev
Ti-Dry	15 μm	173.1	181.1	181.2	189.4
Ti-Coolant		175.8	191.1	197.2	191.1
Increase%		1.6	5.5	8.8	0.9
Ti-Dry	5 μm	182.2	192	185.3	189.1
Ti-Coolant		183.4	193.5	192.9	190.9
Increase%		0.7	0.8	4.1	1.0

Fig. 9 shows FE simulation of cutting process near a pore the size of which is twice of the depth of cut. In the simulation, the formation of protruding chip segments can be confirmed. As tool tip feeds toward pore, the deformation occurs on pore edge close to the tool, while other edge is not influenced (Fig. 9a and b). This results in a kind of disorder in continuous chip generation and induces a big gap inside chips which terminates shear deformation of material leading to the protruding material out of the gap (Fig. 9c and d). It should be noted that when large saw-toothed chips are generated, the location of pore associated with saw-toothed chip formation will affect the chip shape and the timing of protruding generation.

As undeformed chip thickness decreases to $h_{max} = 172$ nm, the effect of pores on chip formation has become more obvious, as shown in Fig. 10. Chip tearing in porous titanium cutting are more significant than those in the cutting of pure titanium. The pores might become sources for chip tearing. The chip tearing phenomenon has a remarkable impact on machined surface topography at extremely small h_{max} [12].

3.3. Machined surface topography

Fig. 11 shows SEM micrographs of the machined surface of porous titanium. It is seen that as h_{max} decreases, more pores are closed. At an extremely small h_{max} (172 nm), almost no open pores are observed on the machined surface (Fig. 11c). Analyzing the SEM images using ImageJ software indicates a surface porosity of ~29% at $h_{max} = 12331$ nm. Fig. 12 shows an example of SEM image processed to calculate the area ratio of surface pores by the ImageJ software. However, the surface porosity decreases to ~1% at $h_{max} = 172$ nm as shown in Fig. 13. During cutting, only the porosity of the surface layer

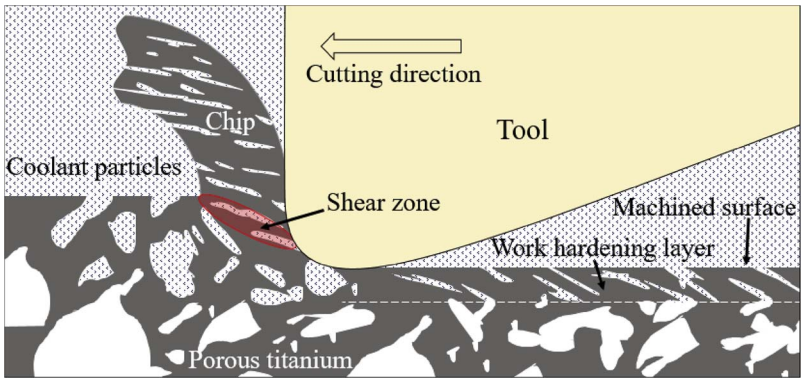

Fig. 17. Schematic illustration of coolant effects.

is changed while the internal region is unaffected, thus the surface porosity evaluated by area fraction is considered in this study instead of volumetric porosity.

Two factors might have affected the phenomenon of pore closing: the high shear stress induced by tool edge, and chips embedding into the pores. The tool-induced high shear stress causes extensive plastic flow of material beneath the tool edge, leading to pore closing. The detached parts of chips might enter the pores and embedded after tool pass, causing pore closing.

Fig. 14 shows FE simulations of cutting behavior around a square-shape pore at two different depths of cuts (a). In this case, the pore is 5 times bigger than the tool edge radius (r). When the tool tip feeds toward an edge of a pore at extremely small undeformed chip thickness (Fig. 14a), the tool-induced high pressure pushes the chip to reach the other side of the pore. Due to high contact pressure, interfacial welding phenomenon occurs between the chip and workpiece surface, which leads to pore closing and boundary generation as shown in Fig. 11b2 and c2. As shown in Fig. 15a, the pressure in the contact area between the chip and the workpiece is more than 500 MPa, which is higher than the yield strength (300 MPa) of pure titanium, and thus able to cause interfacial welding. The torn chip accelerates the process entering chip into pores and welding phenomenon. At higher undeformed chip thickness, however, welding phenomenon does not occur due to the fact that chip generated is more uniform and stress is not concentrated

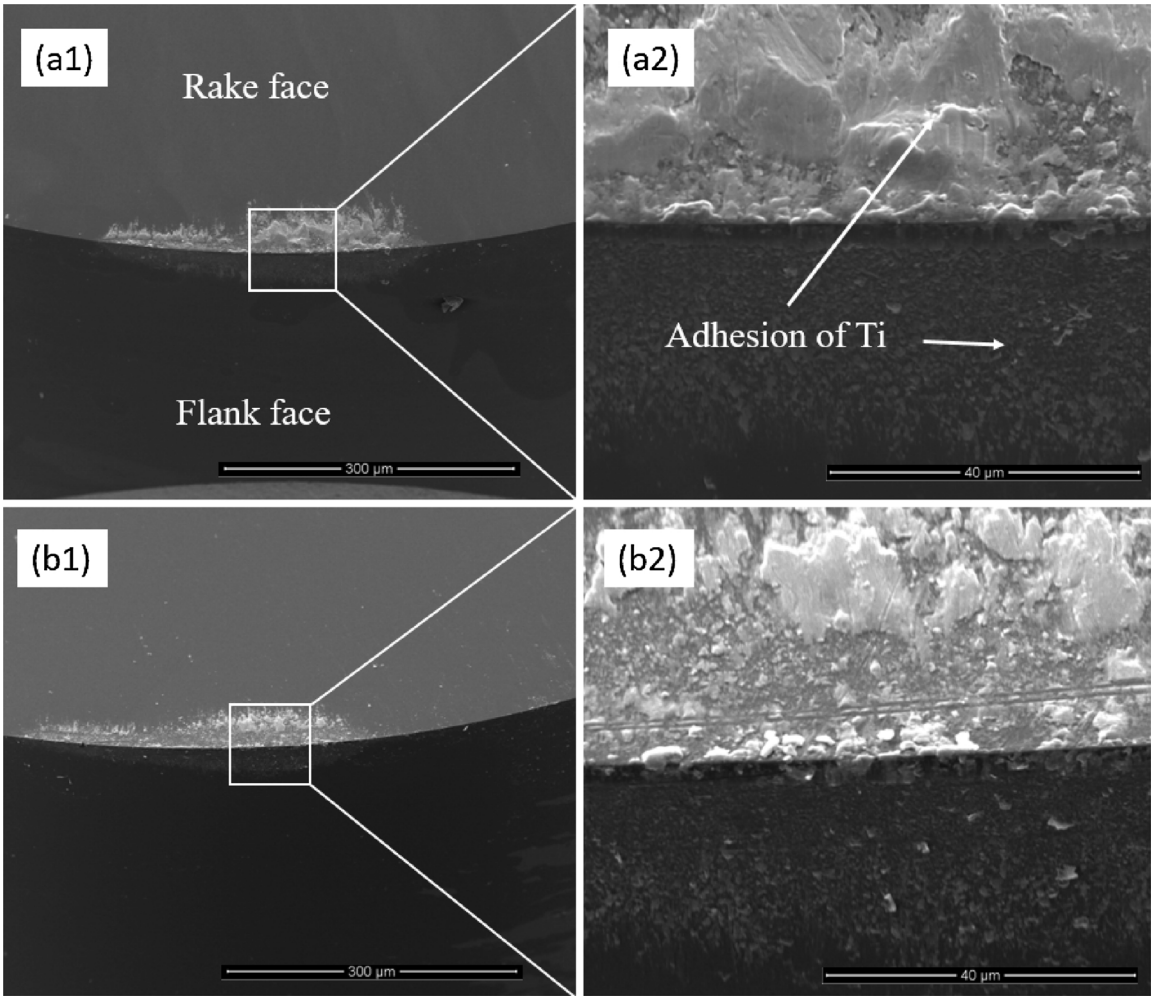

Fig. 18. SEM micrographs of tool tip in cutting of porous titanium for a cutting distance of 100 m at (a) dry (b) wet conditions.

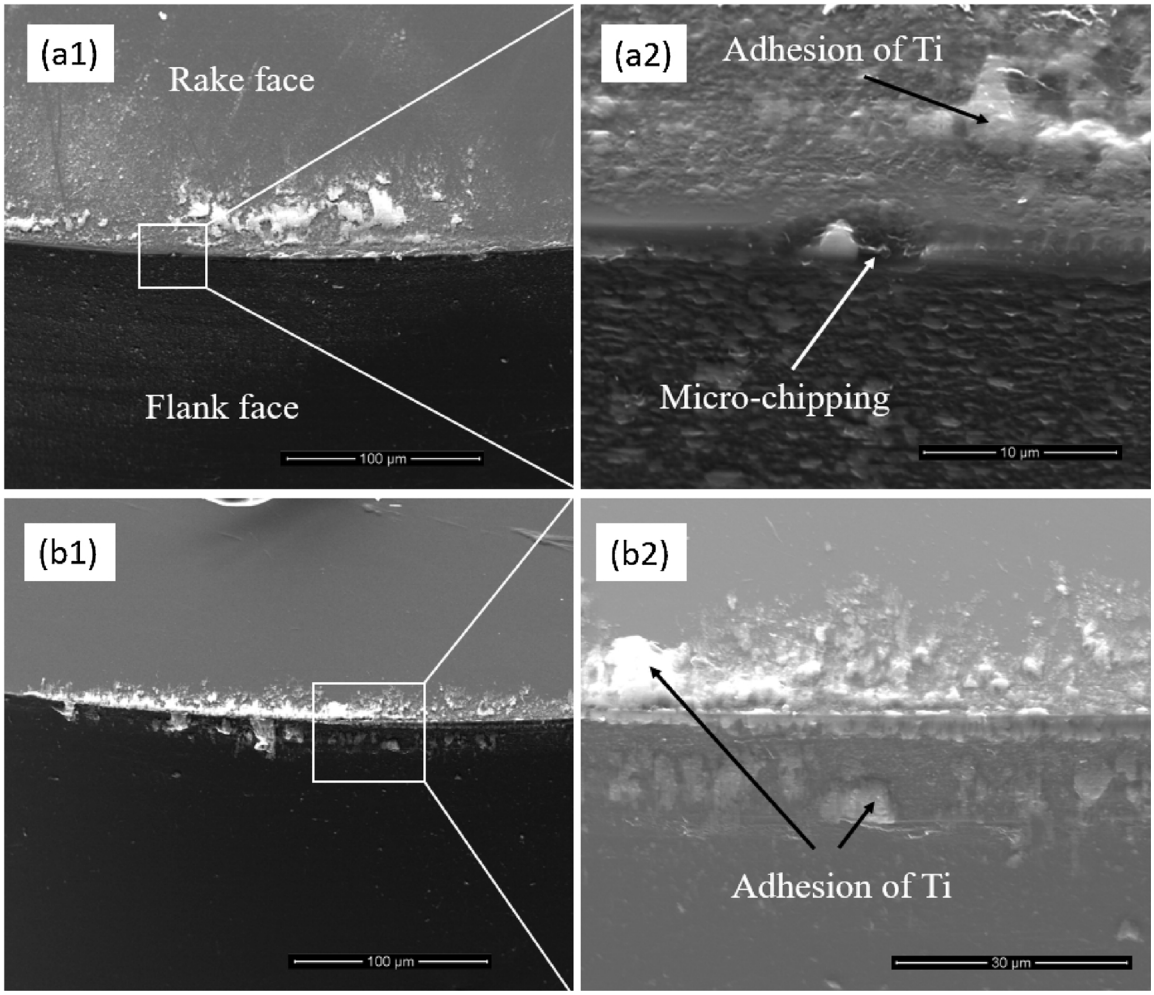

Fig. 19. SEM micrographs of tool tip in cutting of porous titanium for a cutting distance of 1 km at (a) dry (b) wet conditions.

compared to low undeformed chip thickness, thus pores remain open, as shown in Fig. 14b and Fig. 15b.

The welding phenomenon occurring in cutting porous titanium may justify the reason why there is no significant difference in cutting forces between pure titanium and porous titanium at extremely fine undeformed chip thickness (Fig. 3).

3.4. Coolant effects

Fig. 16 shows the results of cutting force measurements during machining of both pure titanium and porous titanium in wet cutting using coolant.

Compared with dry cutting (Fig. 3), wet cutting decreases cutting force slightly. The use of coolant might have two double-face effects on cutting force. One is the lubrication effect, i.e., the coolant can penetrate the pores and lubricate both the tool-workpiece interface and the shear deformation zone along the shear plane, and in turn, decreases cutting forces. The other is the cooling effect on work hardening, which increases cutting forces. Large-strain deformation enhances strength and hardness in machining titanium [23]. This work hardening process will be affected by temperature, so that resulting surface hardness will change with temperature. Using coolant causes rapid cooling and enhances the work hardening effect. Fig. 17 shows a schematic model for coolant effects on the cutting process.

Tables 3 shows the results of micro Vickers hardness for the machined surface of pure titanium at different depths of cuts. The results

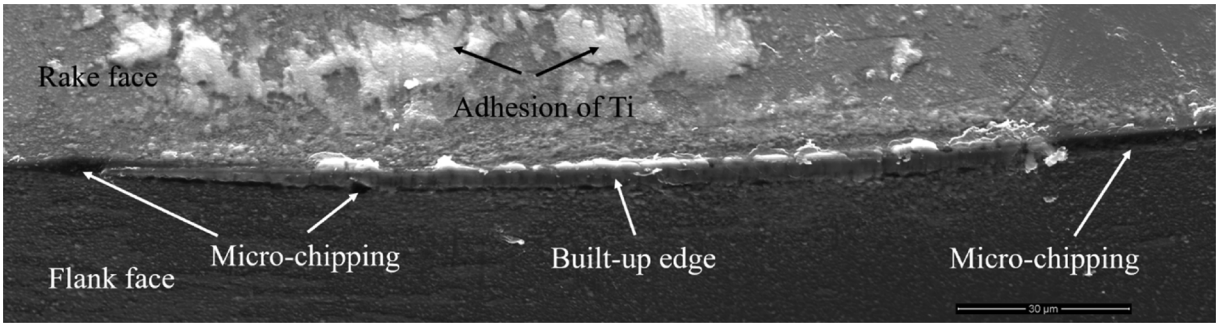

Fig. 20. SEM micrographs of tool tip in cutting of porous titanium for a cutting distance of 2 km at dry condition.

demonstrate that a ~9% increase in surface hardness occurs after wet machining. This phenomenon might be explained by the effect of coolant on cooling rate of the machined surface. Kitagawa et al. [24] recorded a temperature between 800 and 900 °C in cutting area during continuous cutting of titanium alloys at a cutting speed of 50 m/min. After tool passes, the coolant penetrates the fresh surface and increases the cooling rate that may increases surface hardness.

3.5. Tool wear

Fig. 18 is the SEM micrographs of the tool edges after cutting of porous titanium for a cutting distance of 100 m. The h_{max} was changed from 99 nm to 12331 nm during this cutting distance, and 96% of the total cutting distance was performed at a maximum undeformed chip thickness less than 500 nm. As shown in Fig. 18a, material adhesion on the tool face in porous titanium cutting is lower than those in pure titanium cutting [12]. This might be due to the lower density of porous structure and the lower contact pressure at the tool-workpiece interface. Using a coolant helps to lubricate the interfaces of tool rake face and chip, flank face and machined surface, and thus decreases the quantity of material adhesion on those tool faces, as shown in Fig. 18b. Nevertheless, the coolant cannot penetrate into the tool tip region during the cutting process due to the high cutting speed, thus the material adhesion near the cutting edge (tool tip) is almost the same.

In order to investigate tool wear characteristics in porous titanium cutting, the tools were observed for different cutting distances. Before observation, in addition to washing in alcohol, tools were cleaned using an ultrasonic cleaning with acetone to remove any adhering debris.

As shown in Fig. 19a, a micro chipping was observed after a cutting distance of 1 km in dry cutting. The cutting distance for micro chipping occurrence is longer than that of pure titanium cutting at the same condition [12]. Next, experimental tests were repeated in a wet condition by applying the coolant. Observations showed that material adhesion on tool faces sharply decreased compared to dry cutting (Fig. 19b).

As cutting distance increases to 2 km (Fig. 20), the process of forming built-up-edge led to extensive micro chippings and premature failure of the tool. That means the more pores were closed due to higher pressure induced by the dull tool tip during the cutting process. Moreover, the debris adhesion also increased.

The results demonstrate that the tool wear in ultraprecision cutting is concentrated to tool edge, which is different from micrometer-scale cutting where flank wear land and crater wear on rake face are dominant [25–27].

Titanium has high chemical reactivity with many cutting tool materials. As a result, cutting tools wear very rapidly due to the highly localized stress and strong adhesion at the tool-chip interface (rake face) and tool-workpiece interface (flank face) close to tool cutting edge [28,29].

The graphitization of diamond in the cutting of titanium using diamond tool has been investigated by many researchers. They showed that cutting pressure and temperature promote graphitization remarkably [30–33]. In ultraprecision machining, pressure significantly increases as undeformed chip thickness decreases that may cause rising localized stress and accelerate tool wear.

4. Conclusions

The mechanism of cutting and surface integrity in the ultraprecision diamond turning of porous titanium was investigated under various conditions. The following conclusions were obtained:

(1) The presence of pores significantly changes mechanism of cutting in porous titanium compared to pure titanium. The chip morphology and surface topography depend on pore size and location.
(2) At an extremely small undeformed chip thickness, pores smaller than undeformed chip thickness will be closed due to the shear deformation inside chips, while larger pores cause segmentation of chips and protruding lamella. Pores also act as sources for chip tearing and crack propagation.
(3) As undeformed chip thickness decreases, most pores will be closed on the machined surface due to the welding phenomenon, leading to an average porosity drop from ~30% to 1%. Larger pores, however, will remain open on machined surface at a larger undeformed chip thickness.
(4) The use of coolant has double-face effects on cutting force. Coolant penetrates the pores and lubricates the tool-workpiece interface and the shear deformation, and in turn, decreases cutting forces. Using coolant also causes rapid cooling, enhances the work hardening effect and increase machined surface hardness.
(5) Tool wear in cutting porous titanium is suppressed compared with that of pure titanium, especially in wet cutting.

References

[1] Abolghasemi Fakhri M, Bordatchev EV, Tutunea-Fatan OR. An image-based methodology to establish correlations between porosity and cutting force in micromilling of porous titanium foams. Int J Adv Manuf Technol 2012;60:841–51.
[2] Braem A, Van Mellaert L, Hofmans D, De Waelheyns E, Anné J, Schrooten J, et al. Bacterial colonisation of porous titanium coatings for orthopaedic implant applications–effect of surface roughness and porosity. Powder Metall 2013;56:267–71.
[3] Fröjd V, Chávez de Paz L, Andersson M, Wennerberg A, Davies JR, Svensäter G. In situ analysis of multispecies biofilm formation on customized titanium surfaces. Mol Oral Microbiol 2011;26:241–52.
[4] Bram M, Kempmann C, Laptev A, Stöver D, Weinert K. Investigations on the machining of sintered titanium foams utilizing face milling and peripheral grinding. Adv Eng Mater 2003;5:441–7.
[5] Chen S, Head D, Jawahir IS. An investigation of machining performance for controlled surface quality requirements in porous tungsten [for dispenser cathodes]. Fifth IEEE Int. Vac. Electron. Conf. (IEEE Cat. No.04EX786), vol. 52. 2005. p. 358–9.
[6] Schoop J, Effgen M, Balk TJ, Jawahir IS. Improved product quality and resource efficiency in porous tungsten machining for dispenser cathode application by elimination of the infiltration process. In: Nee AYC, Song B, Ong S-K, editors. Re-engineering Manuf. Sustain. Proc. 20th CIRP Int. Conf. Life Cycle Eng. 2013. p. 241–4.
[7] Pusavec F. Porous tungsten machining under cryogenic conditions. Int J Refract Met Hard Mater 2012;35:84–9.
[8] Heidari M, Yan J. Ultraprecision surface flattening of porous silicon by diamond turning. Precis Eng 2017;49:262–77.
[9] Heidari M, Yan J. Fundamental characteristics of material removal and surface formation in diamond turning of porous carbon. Int J Addit Subtractive Mater Manuf 2017;1:23–41.
[10] Yan J, Zhang Z, Kuriyagawa T. Mechanism for material removal in diamond turning of reaction-bonded silicon carbide. Int J Mach Tools Manuf 2009;49:366–74.
[11] Liu K, Li XP, Rahman M, Neo KS, Liu XD. A study of the effect of tool cutting edge radius on ductile cutting of silicon wafers. Int J Adv Manuf Technol 2007;32:631–7.
[12] Heidari M, Yan J. Nanometer-scale chip formation and surface integrity of pure titanium in diamond turning. Int J Adv Manuf Technol 2017. http://dx.doi.org/10.1007/s00170-017-1185-1.
[13] Nakayama K, Tamura K. Size effect in metal-cutting force. J Eng Ind 1968:119–26.
[14] Joshi SS, Melkote SN. An explanation for the size-effect in machining using strain gradient plasticity. J Manuf Sci Eng 2004;126:679.
[15] Shaw MC. A quantized theory of strain hardening as applied to the cutting of metals. J Appl Phys 1950;21:599–606.
[16] Shaw MC. The size effect in metal cutting. Sadhana 2003;28:875–96.
[17] Lovell MR, Cohen P, Menezes PL, Shankar R. Tribological characterization of machining at very small contact areas. J Tribol 2009;131:42201–7.
[18] Subbiah S. Some investigations of scaling effects in micro-cutting. Georgia Institute of Technology; 2006.
[19] Mian AJ, Driver N, Mativenga PT. Identification of factors that dominate size effect in micro-machining. Int J Mach Tools Manuf 2011;51:383–94. http://dx.doi.org/10.1016/j.ijmachtools.2011.01.004.
[20] Ahn IH, Moon SK, Hwang J. An efficient way of investigating the intrinsic size effect in machining. Proc Inst Mech Eng Part B J Eng Manuf 2016;230:1622–9.
[21] Wlesner C. Residual stresses after orthogonal machining of AISI 304: numerical calculation of the thermal component and comparison with experimental results. Metall Trans A 1992;23A:989–96.
[22] Weber M, Hochrainer T, Gumbsch P, Autenrieth H, Delonnoy L, Schulze V, et al. Investigation of size-effects in machining with geometrically defined cutting edges. Mach Sci Technol 2007;11:447–73.
[23] Shankar MR, Rao BC, Lee S, Chandrasekar S, King AH, Compton WD. Severe plastic deformation (SPD) of titanium at near-ambient temperature. Acta Mater 2006;54:3691–700.
[24] Kitagawa T, Kubo A, Maekawa K. Temperature and wear of cutting tools in high-speed machining of Inconel 718 and Ti-6Al-6V-2Sn. Wear 1997;202:142–8.
[25] Jawaid A, Che-Haron CH, Abdullah A. Tool wear characteristics in turning of

titanium alloy Ti-6246. J Mater Process Technol 1999;92–93:329–34.
[26] Da Silva RB, Machado ÁR, Ezugwu EO, Bonney J, Sales WF. Tool life and wear mechanisms in high speed machining of Ti–6Al–4 V alloy with PCD tools under various coolant pressures. J Mater Process Technol 2013;213:1459–64.
[27] Klocke F. Manufacturing processes 1: cutting. Berlin: Springer; 2011.
[28] Hartung PD, Kramer BM, von Turkovich BF. Tool wear in titanium machining. CIRP Ann – Manuf Technol 1982;31:75–80.
[29] Paul E, Evans CJ, Mangamelli A, McGlauflin ML, Polvani RS. Chemical aspects of tool wear in single point diamond turning. Precis Eng 1996;18:4–19.
[30] Thornton AG, Wilks J. Tool wear and solid state reactions during machining. Wear 1979;53:165–87.
[31] Kohlscheen J, Stock H-R, Mayr P. Tailoring of diamond machinable coating materials. Precis Eng 2002;26:175–82.
[32] Ezugwu EO, Bonney J, Yamane Y. An overview of the machinability of aeroengine alloys. J Mater Process Technol 2003;134:233–53.
[33] Qian J, Pantea C, Voronin G, Zerda TW. Partial graphitization of diamond crystals under high-pressure and high-temperature conditions. J Appl Phys 2001;90:1632–7.